

# Arc-length characterization of finite, radial growth patterns

Andreas A. Hennig,<sup>†</sup> Ilaria Beechey-Newman,<sup>†</sup> Natalia Kizilova,<sup>‡,¶</sup> and Erika Eiser<sup>\*,†</sup>

<sup>†</sup>*PoreLab, Department of Physics, Norwegian University of Science and Technology, Høgskoleringen, Trondheim, N-7491, Norway.*

<sup>‡</sup>*Warsaw University of Technology, Institute of Aeronautics and Applied Mechanics, Nowowiejska, 24, Warsaw, 00-665, Poland.*

<sup>¶</sup>*V.N. Karazin Kharkiv National University, Department of Applied Mathematics, Svobody sq., 4, Kharkiv, 61-022, Ukraine.*

E-mail: erika.eiser@ntnu.no

## Abstract

We present a method to characterize the distribution of length-scales of finite, disordered patterns with, on average, radial symmetry. This method makes it possible to quantify the distribution of characteristic length scales in cases where the conventional “linear” chord method does not work. We show that the method can clearly distinguish regular patterns, patterns that are formed by diffusion-limited aggregation, and patterns that form during the slow drying of confined, colloid-laden droplets, explained by Beechey-Newman *et al.*<sup>1</sup> We also introduce a method to find the centre-point of these finite patterns, without assuming a full connectivity in the pattern. The method should be widely applicable to other, finite quasi-two-dimensional patterns.

# Introduction

The so-called “chord-length distribution method”<sup>2</sup> is a convenient tool to characterize the distribution of length scales of clusters and voids in a disordered yet homogeneous, two-dimensional pattern of two phases (*e.g.* solid and air). This chord analysis aims to determine the distributions of segment-lengths of a (any) straight line that intersects a large number of solids and void spaces, *e.g.* in a gel network.<sup>3</sup> The conventional chord analysis does not provide meaningful results for patterns that are not homogeneous and finite. Yet such patterns are important: many quasi-two-dimensional aggregation phenomena yield patterns that are a) finite and b) not homogeneous in space. One example among many is the pattern that is formed by diffusion limited aggregation (DLA). For such, on average radial patterns, chord analysis is not useful. Here we propose a closely related approach, to probe the arc-length distribution of circles that intersect both solid and void domains. Importantly, this arc-length distribution depends on the radius of the intersecting circle, even when averaged over many similar patterns. In what follows, we will refer to this type of analysis as circular chord-length analysis: this name is less precise than arc-length distribution, but stresses the analogy with the conventional chord-length distribution. Arc-length distributions can serve as a “fingerprint” of disordered radial patterns, obtained experimentally as shown in Figure 1. We compare the circular arc-length distribution for three visually different patterns in Figure 3 (a colloidal drying pattern, a diffusion limited aggregation (DLA) pattern, and a “random birthday pie” pattern) to illustrate that the method can be used to quantify the visual differences between these patterns.

## Systems

Roughly radial patterns often form due to the deposition of colloids, either due to evaporation of the solvent, or due to (diffusion-limited or reaction-limited) aggregation of colloids from a colloid-laden suspension. A classic example is the famous “coffee-stain-effect”<sup>4</sup> where the

dispersed coffee grounds mostly accumulate in the rim of the dried stain. The effect was explained in ref. 4 for the case of droplets on partially wetting surfaces, where the droplet circumference gets pinned. As the droplet evaporates, there will be a capillary flow towards the rim, transporting almost all colloidal particles towards the perimeter. In inkjet printing, but also in coatings and paintings, this effect is unwanted, and efforts have been made to overcome the capillary flows that drive deposition on the pinned contact line.<sup>5–8</sup>

More recently, maze-like patterns of slowly evaporating cylindrical droplets were described by Beechey-Newman *et al.*<sup>1</sup> These patterns form inversely-ramified patterns, meaning that the branches in the pattern become thinner towards the centre. In the present paper, we aim to determine and compare “fingerprints” of the various patterns listed above, with those of simpler radial patterns.

The fractal dimension of a pattern is a convenient quantity to characterize naturally-formed radial patterns that are scale-invariant. This fractal dimension can be used to distinguish different growth mechanisms; *e.g.*, viscous fingering, stable displacement or capillary fingers in the invasion percolation of two immiscible fluids in porous media.<sup>9</sup> In contrast, the patterns observed in ref. 1 are *not* scale-invariant: the characteristic length scale of the branches changes rather abruptly with radius, something that does not lend itself for description in terms of a fractal or multi-fractal description. It is for this reason, that for such systems, we explore the angular equivalent of the chord method.

The remainder of this paper is organized as follows: first we introduce the circular arc-length distribution method (CAL), and its relation to the linear chord-length distribution introduced by Méring and Tchoubar.<sup>2</sup> We then consider examples of applications of the CAL method to experimentally observed drying patterns of colloidal droplets, for DLA patterns, and for artificial radial patterns. We show that, for experimental patterns, the CAL method can generate unique fingerprints that depend on the radius of the intersecting circle. Such an analysis is particularly useful in cases where the nature of the pattern formation changes with the radius of the deposit.

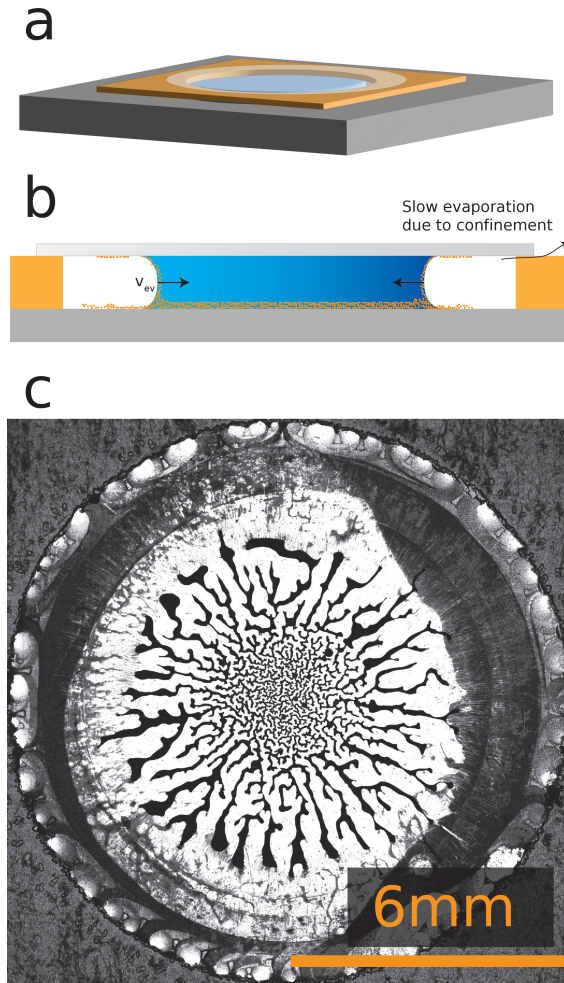


Figure 1: Illustration of the experimental setup from ref. 1 that was used to obtain the colloidal maze-like patterns. A microscope slide is prepared with a double-sided sticky tape, where we punch a hole of  $r = 6$  mm and deposit a droplet of water containing 1 wt.% of  $1 \mu\text{m}$  large TPM-particles, as shown in (a). Then, a cover-slip is placed on top of the circular cell, forcing the evaporation process to take many days. A cross-section of the cell is shown in (b), showing the colloid deposition both on the bottom and top glass plates. The slow evaporation process drives colloids to assemble into a contiguous maze, as seen in the photograph shown in (c).

## Arc-length distributions

The circular arc-length analysis used in this work is a fairly straightforward generalization of the linear chord-length method of Levitz and Tchoubar.<sup>10</sup> In its simplest form, the CAL method is used to characterize biphasic patterns, where the two “phases” might be real

phases of matter, *e.g.*, solid and vapor, or simply different labels (*e.g.*, black and white, characterizing an artificially generated pattern).

We use a fairly standard method to binarize the experimental images, similar to the method used in Zupkauskas *et al.*<sup>3</sup> First, we apply a Gaussian blur on the image, and threshold by Otsu’s method.<sup>11</sup> Finally, a labelling algorithm is used to filter out all clusters below a certain size, to minimize the random labelling errors that inevitably occur.

The first step in the CAL analysis is to determine the centre of the pattern. For natural patterns such as DLA, the choice of the centre is obvious: it is the point where the pattern originated. Conversely, in the case of drying patterns, the centre might be identified with the last point to dry; ideally circles around the central point should correspond to the location of the drying front at different points in time. If the drying proceeds symmetrically, then the last point to dry would be the correct choice for the central point in the CAL analysis, but in general, there is some arbitrariness in choosing the centre of the pattern.

Once the centre of the pattern has been located or chosen, we can draw circles of increasing radius  $r$  around this centre. Typically, such a circle will intersect many boundaries between the two phases (say: “solid” and “void”). If we attribute the value 1 to all points in the solid phase, and 0 to points in the void phase, then we can construct a function  $\mathcal{T}(\theta, r)$ , where  $0 < \theta \leq 2\pi$  is the angle specifying a point on the circle corresponding to radius  $r$ . As  $\mathcal{T}(\theta, r)$  can have only the two values 0 and 1, the resulting function at constant  $r$  looks like a (random) telegraph signal as a function of  $\theta$ . In experiments, the resolution with which the pattern is obtained is limited by the pixel size, typically a square with length and width  $\Delta$ . A pixel “belongs” to a given circle if that circle intersects the pixel area. In general, a pixel might belong to more than one circle. However, if the radii of adjacent circles differ by more than  $\Delta\sqrt{2}$  then every pixel belongs to at most one circle. Of course, the density of pixels on a circle will, in general, not be constant, but in practice that is not a serious problem for determining arc-segment lengths.

In some cases, pixels may have the wrong “label” due to noise. Unless the noise level is

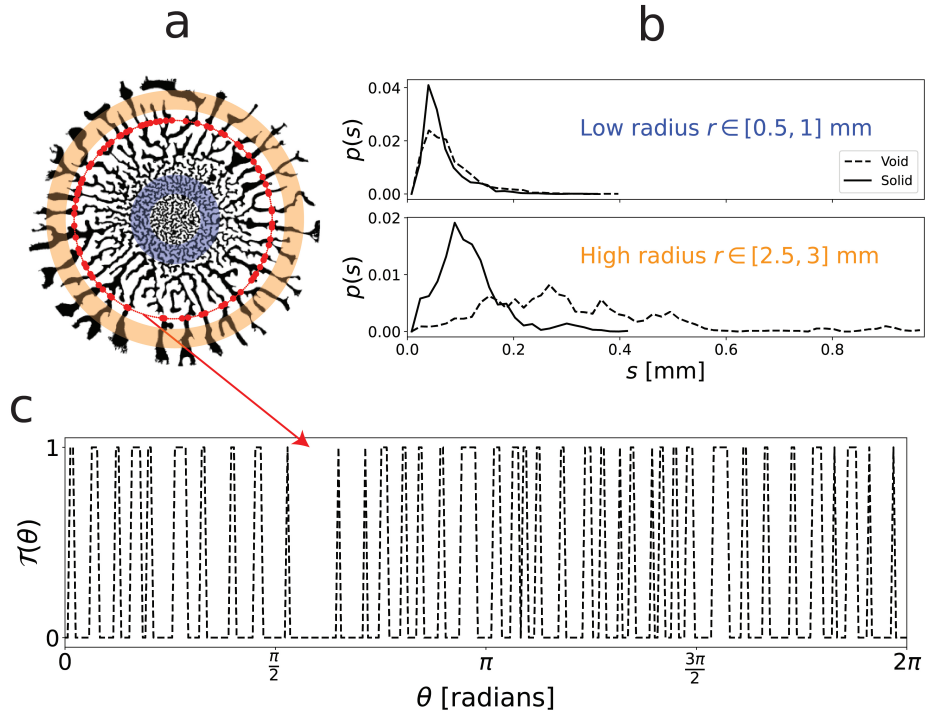


Figure 2: (a) Illustration of the circular arc-length distribution for the colloidal drying pattern P2, that was appropriately cropped and binarized. For a given radius (red circle), each void-solid (white-black) interface is marked with a red dot, allowing us to store the length along the circle between each interface. (b) Resulting distribution of the arc lengths  $s$  between interfaces, where  $p(s)$  is the probability for a given  $s$ . Radii lying in the orange shell show a broader distribution than those lying in the blue, inner shell, with finer structures. (c) Telegraph signal  $\mathcal{T}(\theta)$  obtained from the particular radius illustrated in (a), with  $\theta$  starting from the 3 o' clock position moving clockwise. In the signal, 1 indicate the solid phase and 0 corresponds to the void phase. The details of the CAL distribution differ from sample-to-sample, but the overall characteristics remain the same.

very high, it is unlikely that two or more adjacent pixels will be incorrectly labeled due to noise. To remove incorrectly labeled pixels, one should check if its label differs from that of all its neighbors, *i.e.*, if the pixel is isolated. Such pixels should be removed from the analysis. Of course, this procedure can be refined if necessary. However, a labeling error at a domain boundary cannot be removed in this way. In the cases that we study, the noise levels are so low that such errors should have a negligible effect.

Having thus identified the “random telegraph” signal on a given circle, we can identify arc-segments on the circle where the label remains the same. The arc-length of a segment is defined as the distance in the angle  $\theta$  between two adjacent label changes. Note that, as the pattern in  $\theta$  is periodic with a period  $2\pi$ , the distance between the two boundaries of an arc segment should be defined as the distance (in  $\theta$ ) between a given segment boundary and the *nearest periodic image* of the adjacent boundary.

## Analysis of experimental and synthetic patterns

We tested the CAL method by applying it to the the quasi-2D colloidal drying patterns P1, P2 and P3 in Figure 3. These patterns formed under the conditions explained in Figure 1, which differ qualitatively. In addition, we applied the same circular-arc analysis to a numerically generated two-dimensional diffusion-limited aggregation model and an artificial pattern of random segments, which we refer to as the “random birthday pie” (RBP). As was discussed by Levitz and Tchoubar,<sup>10</sup> DLA patterns yield a power-law distribution of the chord lengths in the void phase:  $p_p(s) \sim 1/s^{d_m-1}$  where  $s$  is the chord length and  $d_m$  is the fractal dimension of the pattern in the void phase. Below, we first apply the circular arc-length analysis to a radial colloidal drying pattern<sup>1</sup> and then compare it to that of a DLA pattern. As the mechanisms by which the drying and DLA patterns form are very different, we might expect that this should result in rather different CAL distributions.

The circular arc-length distributions of the drying pattern P2 are presented in Figure

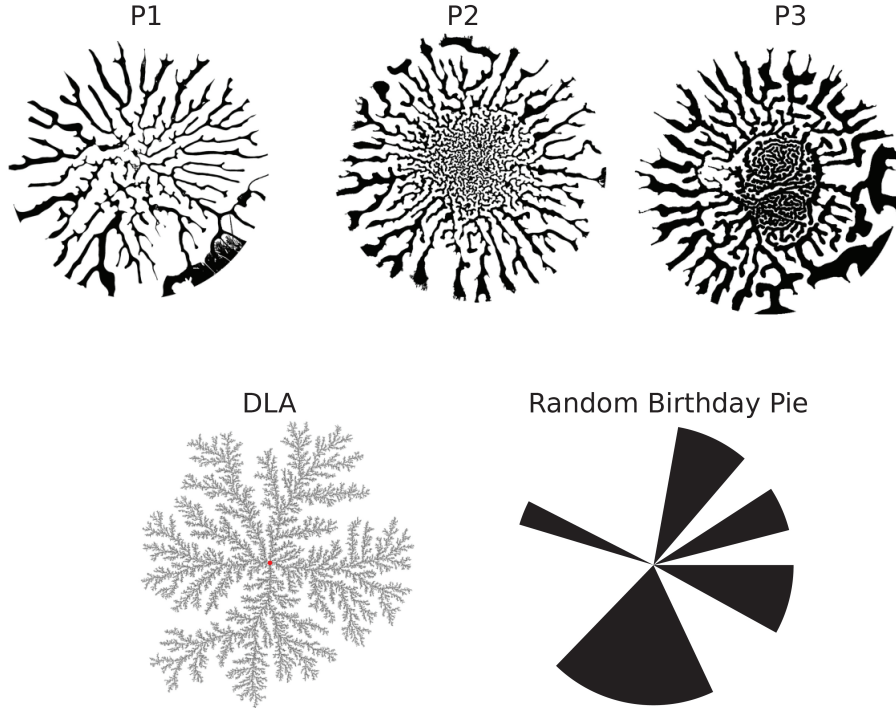


Figure 3: The 5 patterns we compare in this paper, where 3 are drying patterns, obtained by the method described in Figure 1.<sup>1</sup> The images were then appropriately cropped and binarized. The lower two images are that of a DLA pattern, which was generated with 400000 particles in a  $2048 \times 2048$  grid and a RBP pattern, which produces a radially invariant CAL distribution.

2. From this figure we see that the distributions will vary with the radius of the pattern; the goal of the method is to understand these variations. It is instructive to compare our patterns with two characteristic behaviours. In DLA, the finger thicknesses will be 1 pixel, with only a few exceptions. Conversely, a radially invariant pattern, such as the RBP, will have a finger thickness proportional to the radius with a constant determined by the fraction of solid phase in the pattern:  $s = \varphi \cdot r$ .

In the conventional chord length analysis, where we create histograms of cord-lengths in  $x$ - and  $y$ -directions in a porous medium, for instance, we are usually interested in finding an average characteristic length scale. This could be for instance the average pore-size in the system.<sup>3</sup> In our radial analogy, we illustrate the mean arc lengths For the experimentally obtained and artificial patterns in Figure 4. The RBP pattern scales linearly in both phases (with the solid fraction  $\varphi \approx 0.5$  as the slope; turquoise dashed lines). In contrast, the DLA

pattern has a constant solid arc length, while the average *void* arc-length grows as a power-law with the radius (black dashed lines). We find that the drying patterns fall somewhere between the two synthetic patterns. All colloidal drying patterns have on average thicker fingers (*solid phase*) and thicker voids (*void phase*) at the outer radii. The main difference is that the finger thickness and void thickness are comparable close to the centre, but the average void finger thickness grow much faster.

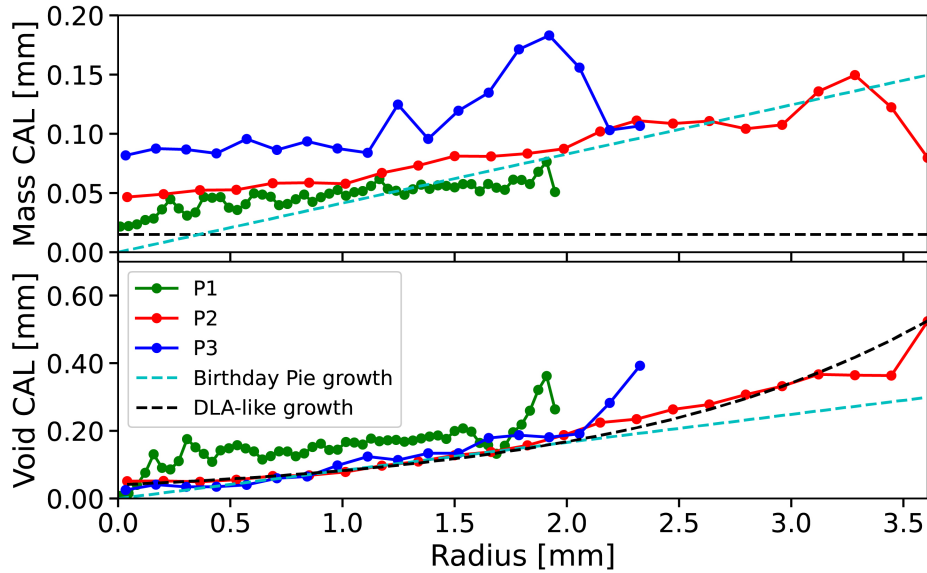


Figure 4: Average arc-lengths of both phases, averaged over  $dr = 20$  pixels, for the 3 drying patterns P1-P3. The growth trends of the synthetic patterns are added as dashed lines for illustration.

We can also explore other properties of the telegraph signal we find in our radial chord length analysis. Starting with the smallest binning length of  $dr = 1$  pixel, we study two properties with respect to the radius. In Figure 5, we present the fraction of the solid phase (*i.e.* by counting the frequency of 1 in the telegraph signal) of the drying patterns at each radius. We expect  $\varphi = 0$  far away where we have a monolayer deposition and therefore do not have any clear fingers;<sup>1</sup> likewise we expect that the centre of the pattern should be in the solid phase, and expect  $\varphi = 1$  as  $r \rightarrow 0$ . All 3 colloidal maze patterns studied display 3 different characteristics in  $\varphi(r)$ : P1 oscillates around a stable value, where the peaks in the oscillations correspond to the radii at which branching occurs; in pattern P2 the solid

fraction increases as the pattern dries; pattern P3 has two fairly sharp jumps with a stable value between them. As these patterns are formed in similar conditions, the instability offer a surprising sensitivity to the subtle differences in the initial conditions.

When inspecting the fingers in a microscope, it is clear that they are fairly uniform in colloid density across the pattern, whereas the space between the fingers contain no colloids. Therefore, measuring the solid and void phases in these images will, to a fairly good approximation, be the same as measuring the mass of the colloidal deposition.

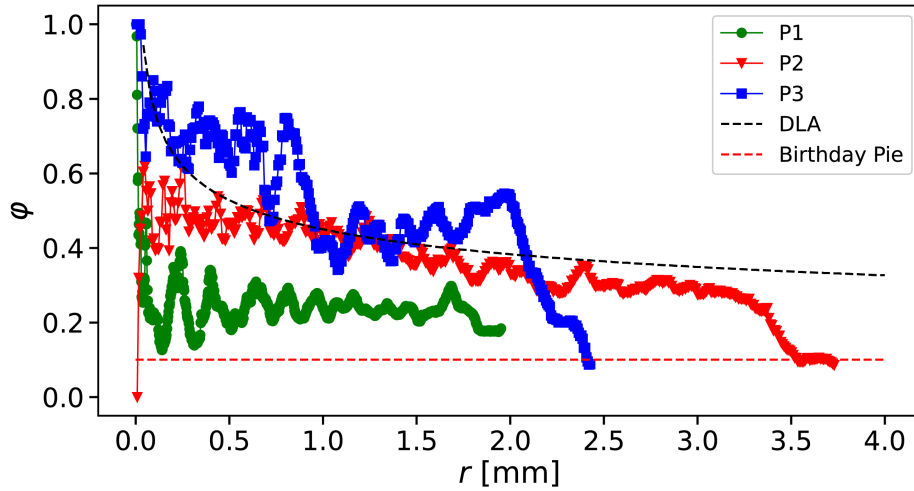


Figure 5: Solid fraction  $\varphi$  along the circular shell of  $dx = 1$  at radius  $r$ . 1 means the shell contains only solid, *e.g.* at the centre of the patterns, while 0 meaning the shell contains only void phase.

At each radius, it is possible to count the number of discontinuous jumps in the telegraph signal. Each of these jumps represents a change in the phase (*i.e.* an interface); the length between phase changes is the arc lengths we study. Thus, counting the number of jumps in the signal is the same as counting the number of distinct arc lengths, and is therefore proportional to the number of fingers, at each radius. The scaling is known for the DLA and Birthday Pie: DLA creates fingers linearly with its growth, while a radially invariant pattern has the same number of interfaces at every radius. The phase jumps of our drying patterns are shown in Figure 6 and display a transition between the characteristic behavior of DLA, close to the centre, and RBP far away from the centre. The fingers clearly merge as

the droplet dries, while the fluid instability causing the fingers also form new fingers during drying. The scaling in region (III) in Figure 6 means the rate of merging roughly matches the rate of forming new fingers. Region (II) marks the transition, where the fingers merge more frequently, and finally, in region (I) the colloidal fingers follow a linear "DLA-like" decay towards the centre.

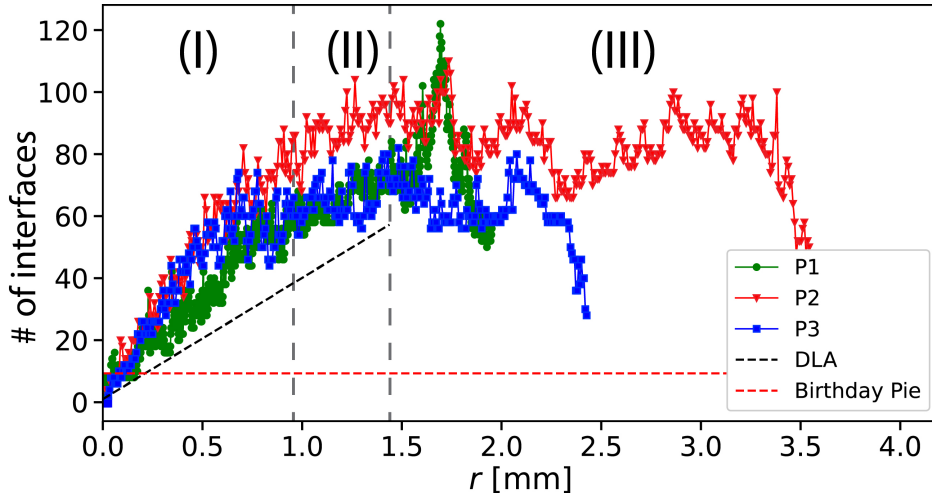


Figure 6: Number of phase shifts of the telegraph signal, corresponding to the surface area the fingers generate. In a DLA, the number of interfaces grows with the circumference, while radially invariant patterns, *e.g.* Random Birthday Pies, have a constant number of phase shifts. We mark this figure with 3 regions where the colloidal patterns exhibit different scaling: Region (III) is characterised with a fairly stable number of interfaces, in region (II) the fingers start merging faster than they are formed, and in region (I) there is a fairly stable merging rate across the drying patterns.

## Using the telegraph signal to find the centre

The choice of the location of the centre of a roughly radially symmetric pattern is to some extent arbitrary. The simplest method to find the centre of mass of a pattern is to locate its center of mass. However, for the colloidal drying patterns, the centre of mass is skewed by the transversal thick fingers forming at the rim of the pattern. These thick fingers tend to form unevenly, hence the centre of mass is clearly different from any visually selected centre. If the pattern is a fully connected network, like a DLA, it is possible to follow the

fingers towards their centre. Following the idea of Horton and Strahlers works on complexity in river networks,<sup>12,13</sup> we may skeletonize a pattern and count the numbers of bifurcations at each node in the skeleton network. However, this method may provide results that are clearly off the centre, as it a) requires a fully contiguous pattern and b) cause arbitrariness where there are multiple equally ordered points.

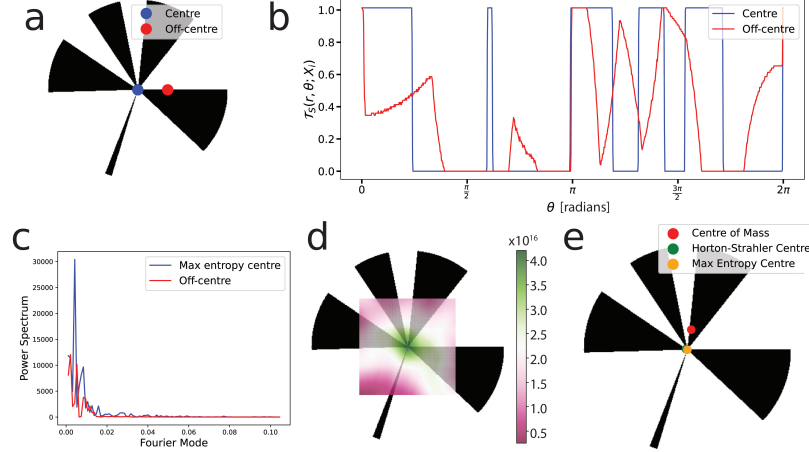


Figure 7: (a)-(c): A comparison of two points, where one is in the centre of the Random Birthday Pie pattern and the other is placed 50 pixels to the right, as shown in (a). (b) compares the summed and normalised telegraph signal  $\mathcal{T}_S(\theta; X_i)$  from the two points, and (c) is their respective power spectra, which is used to calculate the entropy. (d) shows a map of the calculated entropies at each point in the selected window, and (e) shows the centre calculated with 3 different methods.

In order to solve the arbitrariness of deciding the centre, we propose a method using the arc-length distribution. First, we define a test centre  $X_t$ , where we may use any of the mentioned approaches as a first approximation. We define a window of  $N \times N$  pixels centred around  $X_t$ . We then decide the range of relevant radii,  $r \in [r_{\min}, r_{\max}]$ . For each pixel,  $X_i$  within the window, we sum the telegraph signal as

$$\mathcal{T}_S(\theta; X_i) = \frac{1}{r_{\max} - r_{\min}} \int_{r_{\min}}^{r_{\max}} \mathcal{T}(r, \theta; X_i) dr.$$

We then calculate the power spectrum of the signal as  $G(\hat{\theta}) = \int_0^\infty |\mathcal{T}_S(\theta; X_i)|^2 d\theta$ , where  $\hat{\theta}$  denotes the Fourier mode of the angle. A clear periodicity in the summed telegraph signal

will result in a sharp peak in the power spectrum. We therefore use the power spectrum to define an information entropy, as  $S(X_i) = \int_0^\infty G(\hat{\theta}; X_i) \ln G(\hat{\theta}; X_i) d\hat{\theta}$ . The best centre, based on our information entropy, is simply picked as the extremal point  $X_c = \max(S(X_i))$ . Figure 7a-c shows a comparison of two potential centres for the RBP figure, along with their power spectra. Summing the spectra as an entropy, we obtain the map in Figure 7d. In Figure 7e the comparison between the maximum entropy, centre of mass and Horton-Strahler approaches shows that our maximum entropy determination of the figure's centre is the most accurate.

The RBP and DLA patterns have well-defined centres, so we may quantify the errors; these are presented in Table 1.

Table 1: Comparison of the errors we find in the centre of mass and entropy methods. For the DLA we use 20 generated patterns of 100000 particles and a max radius of 1024 pixels. For the Random Birthday Pie we generate 20 random patterns with 10 fingers and a max radius of 150 pixels.

	Centre of Mass	Entropy
DLA	9.53 px	22.34 px
RBP	16.92 px	0.84 px

To find the best centre to apply our CAL analysis of samples P1 and P2 are not as straight forward. Depending on experimental parameters such as possible pinning centres on the support surfaces or on how the samples are levelled horizontally, the apparent centre may not be located at the centre of the sample chamber. However, we can choose a centre by eye and then obtain the maps of the local entropies. These are shown, along with a comparison with other methods in Figure 8. Clearly, the green region is most representative of the true centre of the labyrinthian pattern of our samples. Hence our maximum entropy approach helps to find the best centre, around which the resulting CAL analysis delivers most reliable results for comparisons with other growth laws.

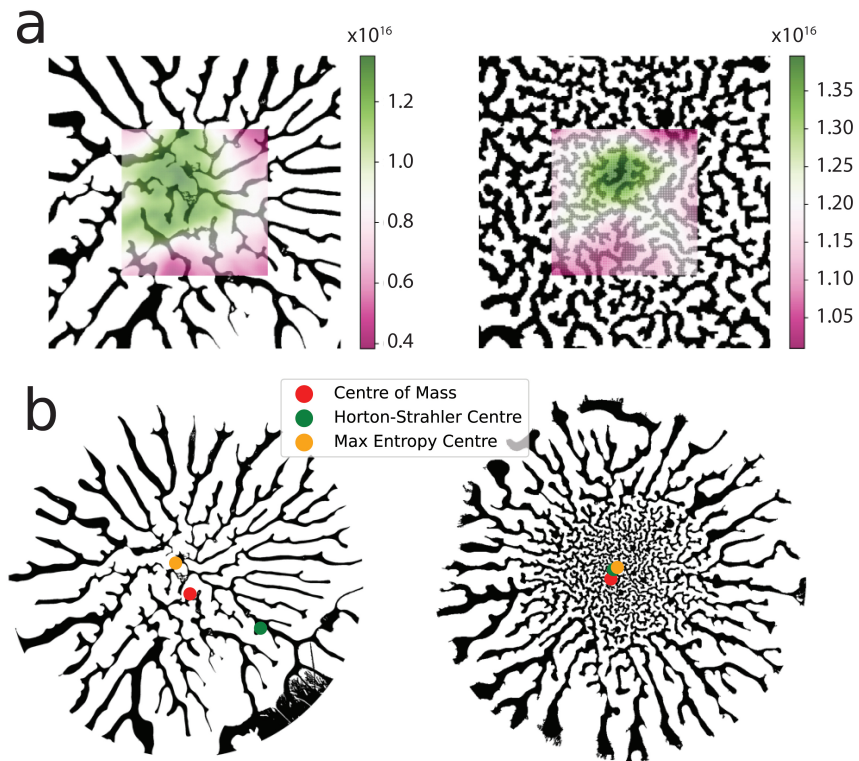


Figure 8: (a) Resulting entropy map of patterns P1 and P2, using the method presented in this paper. (b) Resulting centre points, compared with the two alternative methods.

## Conclusions

We find that extending the traditional chord length distributions to roughly radially symmetric patterns enable us to characterize these patterns in a way that is not feasible with the traditional method. The distributions may serve as a fingerprint of the patterns, which vary from experiment to experiment, due to the subtle differences in the exact initial conditions.

We find that the colloidal drying patterns P1-P3 fall somewhere between the characteristic DLA and Random Birthday Pie patterns. Most importantly, we find the competition between the generation and merging of fingers sustains a fairly stable number of fingers, up to a point where the fingers merge more rapidly. Finally, we use the arc lengths to map an information entropy on the pattern, which we may use to pick a centre where this is not trivial.

The method can be applied to patterns that are not simply radially invariant or self-similar, but fall somewhere between the two.

## Acknowledgement

This work was supported by the Research Council of Norway through its Center of Excellence funding scheme, project number RCN 262644. The authors would like to thank Daan Frenkel for fruitful discussions and extended help in writing this manuscript.

## References

- (1) Beechey-Newman, I.; Kizilova, N.; Hennig, A. A.; Flekkøy, E. G.; Eiser, E. Confined colloidal droplets dry to form circular mazes. Proceedings of the National Academy of Sciences **2025**, *122*, e2508363122.
- (2) Méring, J.; Tchoubar, D. Interprétation de la diffusion centrale des rayons X par les systèmes poreux. I. Journal of Applied Crystallography **1968**, *1*, 153–165.

- (3) Zupkauskas, M.; Lan, Y.; Joshi, D.; Ruff, Z.; Eiser, E. Optically Transparent Dense Colloidal Gels. Chemical Science **2017**, 8, 5559–5566.
- (4) Deegan, R. D.; Bakajin, O.; Dupont, T. F.; Huber, G.; Nagel, S. R.; Witten, T. A. Capillary Flow as the Cause of Ring Stains from Dried Liquid Drops. Nature **1997**, 389, 827–829.
- (5) Hu, H.; Larson, R. G. Marangoni Effect Reverses Coffee-Ring Depositions. The Journal of Physical Chemistry B **2006**, 110, 7090–7094.
- (6) Abdulsahib, A. A.; Mahmoud, M. A.; Aris, H.; Gunasekaran, S. S.; Mohammed, M. A. An Automated Image Segmentation and Useful Feature Extraction Algorithm for Retinal Blood Vessels in Fundus Images. Electronics **2022**, 11, 1295, doi:10.3390/electronics11091295.
- (7) Majumder, M.; Rendall, C. S.; Eukel, J. A.; Wang, J. Y. L.; Behabtu, N.; Pint, C. L.; Liu, T.-Y.; Orbaek, A. W.; Mirri, F.; Nam, J.; Barron, A. R.; Hauge, R. H.; Schmidt, H. K.; Pasquali, M. Overcoming the “Coffee-Stain” Effect by Compositional Marangoni-Flow-Assisted Drop-Drying. The Journal of Physical Chemistry B **2012**, 116, 6536–6542.
- (8) Li, Y.; Diddens, C.; Segers, T.; Wijshoff, H.; Versluis, M.; Lohse, D. Evaporating droplets on oil-wetted surfaces: suppression of the coffee-stain effect. Proceedings of the National Academy of Sciences **2020**, 117, 16756–16763.
- (9) Hansen, A.; Flekkøy, E. G.; Feder, J. Physics of Flow in Porous Media; Cambridge University Press: Cambridge, 2022.
- (10) Levitz, P.; Tchoubar, D. Disordered Porous Solids : From Chord Distributions to Small Angle Scattering. Journal de Physique I **1992**, 2, 771–790.

- (11) Otsu, N. A Threshold Selection Method from Gray-Level Histograms. IEEE Transactions on Systems, Man, and Cybernetics **1979**, 9, 62–66.
- (12) Horton, R. E. Erosional Development of Streams and Their Drainage Basins; Hydrophysical Approach to Quantitative Morphology. GSA Bulletin **1945**, 56, 275–370, doi:10.1130/0016-7606(1945)56[275:EDOSAT]2.0.CO;2.
- (13) Strahler, A. N. Quantitative analysis of watershed geomorphology. Transactions American Geophysical Union **1957**, 33, 913–920, doi:10.1029/TR038i006p00913.